Bulletin of Earthquake Engineering (2020) 18:4705–4724
https://doi.org/10.1007/s10518-020-00874-4

ORIGINAL RESEARCH

# Damage-based yield point spectra for sequence-type ground motions

Yongqun Zhang[1,2] · Jiaxu Shen[1] · Jun Chen[1]

Received: 11 December 2019 / Accepted: 19 May 2020 / Published online: 26 May 2020


**Abstract**
Structural damage caused by mainshock can further be aggravated by aftershocks, which can lead to structural collapse. The current practices on the seismic design of structures generally only consider mainshock effects. This manuscript therefore presents the investigation on damage-based yield point spectra (YPS) of a single-degree-of-freedom (SDOF) system under sequential earthquakes. The collected sequence-type ground motions are recorded from 16 earthquake events and classified to four classes. The aftershocks in sequence are scaled according to different relative intensity levels. The modified Park-Ang model, which consists of maximum displacement and hysteretic energy dissipation, is employed to calculate YPS. The effects of period, ductility factor, damage index, site category, aftershock intensity, and structural damping are statistically studied. The results prove that the strong aftershock ground motion has more distinct influences on the YPS. In particular, the yield strength coefficient demand under seismic sequence increases by 10%–50%. The yield strength coefficient demand determined by the damage-based YPS is greater than that determined by the ductility-based YPS—the former is 10%–40% higher than the latter. Finally, the empirical expression of damage-based YPS is established by statistical mean method and regression analysis.

**Keywords** Yield point spectra · Sequence-type ground motions · Damage index · Structural performance

## 1 Introduction

Since the 1990s, several major earthquake disasters have made the world's earthquake engineering community keenly aware that under strong earthquakes, particularly those that exceed the design strength of structures, can severely damage buildings designed with the force-based method. As a result, grave economic losses have been sustained, and the

✉ Jun Chen
cejchen@tongji.edu.cn

1 Department of Structural Engineering, College of Civil Engineering, Tongji University, Shanghai, People's Republic of China

2 Shanghai Key Laboratory of Engineering Structure Safety, Shanghai Research Institute of Building Sciences Co. Ltd, Shanghai, People's Republic of China

seismic design concept that is based solely on ensuring life safety cannot meet the needs of social development. Compared with the force-based design, the displacement-based design focuses on displacement as the design target. Displacements can better reflect the non-linear response of structures that experience strong earthquakes and can well control the functional state of structures during earthquakes. The displacement-based seismic design method has therefore been extensively developed (Moehle 1992; Kowalsky et al. 1995; Chopra and Goel 2001; Rossetto and Elnashai 2005; Powell 2008; Kowalsky et al. 2010). Currently, the widely used seismic design approach, which can achieve displacement-based structures, is the modified capacity spectrum method proposed by Chopra and Goel (1999), and Fajfar (2000). In this method, first, the capacity curve of structures is obtained by non-linear static analysis, and the multi-degree-of-freedom system is transformed into an equivalent single-degree-of-freedom (SDOF) system. Second, the acceleration–displacement response spectrum, which uses spectral acceleration and spectral displacement as vertical and horizontal coordinates on the same graph, represents the capacity and displacement demands, respectively. The seismic demand spectrum can thereafter be obtained by reducing the elastic spectrum using a strength reduction factor. Finally, the system displacement response is solved by the intersection of the capacity and demand curves. Aschheim and Black (2000), Aschheim (2002), Tjhin et al. (2007) analyzed axially loaded members, cantilever shear wall subjected to lateral forces, multi-layer shear wall structure, and bending frame. It was found that the yield displacement ($\Delta_y$) of the structure is a relatively stable parameter. The yield point spectra (YPS), a variant of the capacity spectrum method, are thus proposed. In lieu of period, the relatively stable yield displacement is used as the initial design parameter in the YPS method. The method determines the strength demand of structures by directly controlling the structural ductility demand or peak displacement response that achieves various expected performance levels. Some researchers (Safar and Ghobarah 2008; Kotsoglou and Pantazopoulou 2009) used the YPS method to analyze the maximum impact of structures during earthquakes; the results have fewer errors than the dynamic time history analysis results. The YPS can be used not only for structural performance evaluation, but also for structural design. For example, Tabatabaei and Rahmanian (2012) designed a frame structure with the YPS method.

After the mainshock causes damage to the structure, the aftershocks usually further increase the degree of structure damage. The compounding effect of damage and disruption caused by seismic sequence results in tremendous losses to society, as exemplified by the aftermaths in Wenchuan (2008), Wang (2008), Christchurch (2010–2011), Moon et al. (2014), Tohoku (2011), Kazama and Noda (2012), and Nepal (2015), Chen et al. (2017). Understanding the sequence-type ground motion and its impact on structure response is therefore crucial to the improvement of structure resilience.

Currently, researchers have investigated the influence of aftershocks on structural damage in different ways. Some researchers focused on the effects of seismic sequence on inelastic spectra for structural design, such as the strength reduction factor $R$ spectra (Hatzigeorgiou 2010a; Zhai et al. 2015; Sun et al. 2016), structural damage $D$ spectra (Zhai et al. 2013), and ductility factor $\mu$ spectra (Hatzigeorgiou 2010b; Goda and Taylor 2012). In addition, several investigations studied changes in structural response, e.g., response of reinforced concrete structures (Raghunandan et al. 2015; Efraimiadou et al. 2013; Shen et al. 2019) steel frame buildings (Li and Ellingwood 2007; Ruiz-García and Negrete-Manriquez 2011), and wood frame building (Goda and Salami 2014; Nazari et al. 2015), subjected to sequence-type ground motions. The results in the above investigations prove that larger maximum displacements or more severe structural damage because of seismic sequence compared to those caused by mainshock. Therefore, the influence of aftershock should be considered in the structural design stage. Unfortunately, most current seismic design codes around the world are designed for single earthquake without considering the influence of aftershock.

As previously mentioned, aftershocks aggravate structural damage. The current capacity spectrum and YPS, however, do not reflect the effect of aftershock. Therefore, this manuscript studies the damage-based YPS through numerical analysis of serial nonlinear SDOF systems subjected to sequence-type ground motions. The aftershock ground motions are scaled to have different intensity levels. The influences of period, ductility factor, damage index, site category, aftershock intensity, and structural damping on the YPS are statistically studied. Finally, a predictive model of damage-based YPS is established by statistical mean method and regression analysis.

## 2 Selected sequence-type ground motions

The actual sequence-type ground motion may contain one or more aftershock ground motions. Studies have shown that different numbers of aftershock ground motions increase the structural damage to varying degrees, and the cumulative damage effect may be more severe with the increase in number of aftershock ground motion (Zhai et al. 2013; Goda and Taylor 2012; Li and Ellingwood 2007). In order to facilitate the comparative analysis, the sequence-type ground motion selected in this manuscript is composed of an aftershock ground motion and a corresponding mainshock ground motion.

Researchers have conducted related studies on the sequence-type ground motion. The available ground motion data for research, however, is insufficient because of limited seismic data. Most of these studies thus use artificial ground motion (Raghunandan et al. 2015) or repetitive ground motion (Hatzigeorgiou and Beskos 2009; Hatzigeorgiou and Liolios 2010), but the use of these ground motions may result in significant overestimations of structural drift demands (Ruiz-García and Negrete-Manriquez 2011). The recorded sequence-type ground motions used in this study are therefore selected from the Pacific Earthquake Engineering Research Center (PEER) Next Generation Attenuation (NGA) relationships database (Pacific Earthquake Engineering Research Centre 2018) and strong-motion seismograph networks (K-NET, KiK-net) (National Research Institute for Earth Science and Disaster Resilience 2018). The selection principles are as follows.

(1) The earthquake magnitudes of mainshock and aftershock are not less than 6.0 and 5.0, respectively, excluding earthquakes that are less probable to cause severe damage to the building structure.
(2) The fault distance is greater than 10 km to reduce the influence of near-field effect.
(3) All records should originate from the same station and the same seismic event. The peak ground acceleration (PGA) of mainshock is larger than 0.10 g, while the PGA of aftershock is larger than 0.05 g.
(4) To ensure that the structure is at rest before the aftershocks occur, a 100 s time interval is added between the selected mainshock and aftershock ground motions.
(5) To study the influence of site class on the YPS, ground motions are classified using the site classification method of the United States Geological Survey.

Based on the selection principle, 342 recorded sequence-type ground motions (154 for site class B and 188 for site class C) are chosen from 16 earthquakes, as summarized in

**Table 1** Information of collected sequence-type ground motions

| Earthquake event | Mainshock | | Aftershock | | Number | |
|---|---|---|---|---|---|---|
| | Time | $M_W$ | Time | $M_W$ | Site B | Site C |
| Managua, Nicaragua | 1972-12-23, 06:29 | 6.2 | 1972-12-23, 07:19 | 5.2 | 0 | 2 |
| Imperial Valley | 1979-10-15, 23:16 | 6.5 | 1979-10-15, 23:19 | 5.0 | 0 | 26 |
| Mammoth Lakes | 1980-05-25, 16:34 | 6.1 | 1980-05-25, 16:49 | 5.7 | 2 | 4 |
| Coalinga | 1983-05-02, 23:42 | 6.4 | 1983-05-09, 02:49 | 5.1 | 0 | 2 |
| Chalfant Valley | 1986-07-21, 14:42 | 6.2 | 1986-07-21, 14:51 | 5.6 | 1 | 0 |
| Kalamata, Greece | 1986-09-13, 17:25 | 6.2 | 1986-09-15, 11:41 | 5.4 | 1 | 0 |
| Whittier Narrows | 1987-10-01, 14:42 | 6.0 | 1987-10-04, 10:59 | 5.3 | 6 | 14 |
| Superstition Hills | 1987-11-24, 05:14 | 6.2 | 1987-11-24, 13:16 | 6.5 | 0 | 2 |
| Northridge | 1994-01-17, 12:31 | 6.7 | 1994-01-17, 12:32 | 6.1 | 14 | 13 |
| Umbria Marche | 1997-09-26, 09:44 | 6.0 | 1997-10-03, 08:55 | 5.3 | 8 | 4 |
| Chi Chi | 1999-09-20 | 7.6 | 1999-09-20, 17:57 | 5.9 | 49 | 36 |
| Wen Chuan | 2008-05-12, 14:28 | 7.9 | 2008-05-12, 19:11 | 6.1 | 12 | 7 |
| L'Aquila | 2009-04-06, 01:33 | 6.3 | 2009-04-07, 17:47 | 5.6 | 9 | 0 |
| New Zealand | 2010-09-03, 16:35 | 7.0 | 2011-02-21, 23:51 | 6.2 | 9 | 33 |
| East Japan Earthquake | 2011-03-11, 13:46 | 9.0 | 2011-03-11, 15:15 | 7.7 | 32 | 29 |
| Kumamoto | 2016-04-14, 21:26 | 6.2 | 2016-04-16, 01:25 | 7.0 | 11 | 16 |
| | Total | 154 | 188 | | | |

Table 1. The number of seismic sequences that meet the selection principle is very small on the site class A and D, and unable to perform relevant statistical analysis. To facilitate statistical analysis, the PGA of mainshock in all selected seismic sequences is adjusted to 0.2 g.

The relative intensity of aftershock ground motion ($\gamma$) is defined as

$$\gamma = \frac{PGA_{as}}{PGA_{ms}} \tag{1}$$

where $\mathrm{PGA}_{\mathrm{as}}$ and $\mathrm{PGA}_{\mathrm{ms}}$ are the PGA of the aftershock and the mainshock ground motion, respectively. Parameter $\gamma$ represents the ratio of $\mathrm{PGA}_{\mathrm{as}}$ to $\mathrm{PGA}_{\mathrm{ms}}$. The intensity of the former is generally lower than that of the latter because of the aftershock's lower magnitude. In seismic sequences in the past, however, aftershock with intensities greater than those of mainshock exist. To investigate the influence of aftershocks on YPS therefore, this manuscript adopts 5 levels of $\gamma$: $\gamma$=0.5, 0.8, 1.0, 1.2, and 1.5. In order to provide a design tool that considers different intensity of aftershock ground motions that exist in recorded sequence-type earthquake, the value of $\gamma$ (i.e., 1.5) is used to simulate the extreme case of aftershock.

## 3 Structural damage and performance level

Maximum displacement is common indicator used in performance-based seismic assessment methods, such as performance-based frameworks employed in FEMA-356. The structural damage caused by earthquakes, however, has various forms. The degree of structural damage cannot be fully presented through maximum displacement only. Reasonable indicators must therefore be used to evaluate the degree of structural damage. The structural seismic response is related to the characteristics of the ground motion (amplitude, duration, spectrum, etc.), aftershocks may greatly increase the duration of ground motions and may cause low-cycle fatigue damage to structures, and this situation can be considered by the hysteretic energy. At present, it is generally believed that the maximum deformation and hysteretic energy of the structure are the main factors of structural damage. Two-parameter damage models are accordingly proposed. The widely known Park and Ang damage model, which was initially defined by Park and Ang (1985) and modified later by Kunnath et al. (1992), is employed in the present study. This damage model consists of a linear combination of normalized maximum displacement and hysteretic energy dissipation. The damage index $D$ is expressed as

$$D=\frac{\mu_m - 1}{\mu_u - 1}+\beta\frac{E_h}{F_y\mu_u x_y} \tag{2}$$

where $\mu_m$ is the maximum ductility factor under earthquake ground motion, $\mu_u$ is the ultimate ductility capacity under monotonic loading, $E_h$ is the cumulative hysteretic energy dissipation under earthquake ground motion, $F_y$ and $x_y$ is the yield strength and yield displacement, respectively. $\beta$ is the energy dissipation factor and represents the rate of accumulated damage through hysteretic energy induced by cyclic loading, the value of $\beta$ is 0.1 to represent frame structures (Negro 1997; Lu and Wei 2008) in this manuscript.

To associate the structural performance levels and damage index range, the structural performance level and damage index of the modified Park-Ang model should first be determined. In terms of structural performance level, several versions of performance definition exist. Five performance levels with descriptive damage extent and proposed damage index limits are adopted, namely *Operational*, *Immediate Occupancy*, *Damage Control*, *Life Safety*, and *Collapse Prevention* (Zhang et al. 2017). It is generally demonstrated that $D=(0.4–0.5)$ is the repairable and unrepairable damage boundary proposed by the modified Park-Ang model, whereas $D$ that approaches 1.0 represents total collapse. By associating the damage levels with the available calibration results of the modified Park–Ang model, the range of the damage index for each performance level may be obtained as summarized in Table 2.

**Table 2** Relationship among the performance levels, damage index ranges and degree of damage (Zhang et al. 2017)

| Performance level | Damage index range | Degree of damage |
|---|---|---|
| Operational | $<0.1$ | Negligible |
| Immediate Occupancy | 0.1–0.2 | Minor |
| Damage control | 0.2–0.5 | Moderate |
| Life Safety | 0.5–0.8 | Severe |
| Collapse prevention | 0.8–1.0 | Near collapse |
| Loss of building | $>1.0$ | Collapse |

## 4 Construction procedure of yield point spectra (YPS)

### 4.1 YPS descripion

The YPS can be used to determine the strength demand to limit the peak ductility factor and drift responses of the structure. The yield point spectra plot the yield point of a single-degree-of-freedom system that has a constant displacement ductility factor ($\mu$) for a range of periods on the axes of yield strength coefficient ($C_y$) and yield displacement ($\Delta_y$). The yield strength coefficient is the ratio of the yield strength of the system ($V_y$) to its weight ($W$), and the ductility factor ($\mu_u$) is the ratio of the peak displacement of the system ($\Delta_u$) to its yield displacement.

Figure 1 plots the values of $C_y$ versus $\Delta_y$ for the classic 1940 NS El Centro ground motion for $\mu_u = 1$, 2, 3, 4, 6, 8, and 10. In this case, an ideal elastic–plastic load–deformation relationship is used; viscous damping is 5% of critical damping. When $\mu_u$ is 1, the YPS curve is the same as the capacity spectra curve. When $\mu_u$ has values higher than 1, the curves differ because the YPS and capacity spectra plot $\Delta_y$ and $\Delta_u$, respectively. For the YPS, periods are constant along the radial lines extending from the origin.

### 4.2 Determination of damage-based YPS

Depending on the information available, an exact or approximate method can be used to determine the YPS. If a ground motion time series is available, the strength demand that corresponds to various ductility demands can be exactly determined, as shown by the curves in Fig. 1. Alternatively, if only the elastic response spectrum is available, then the strengths for the specified ductility demands can be approximately determined conventionally using a smooth $R$–$\mu$–$T$ relationship. This follows the same idea expressed by Chopra and Goel (1999) and Fajfar (2000) with the improvement of the seminal capacity spectra method (Freeman 1978), from which all these methods are derived. Considering the impact of cumulative damage on strength demand, the $R$–$\mu$–$D$–$T$ relationship is employed to determine the strength that corresponds to various ductilities (Zhang et al. 2017). In the calculations, the yield displacement corresponding to a given period and strength is determined using a simple relationship:

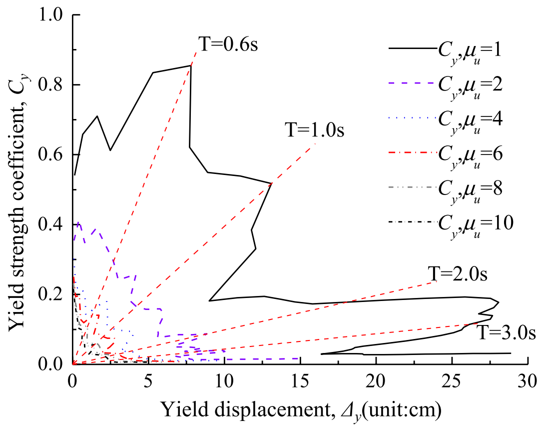


**Fig. 1** Yield point spectra calculated for the 1940 NS El centro record

$$\Delta_y = \left(\frac{T}{2\pi}\right)^2 S_a \tag{3}$$

where $T$ is the natural period of the SDOF system; $S_a$ is the pseudo-acceleration, given equivalently by $C_y g$; $g$ is the acceleration of gravity.

In the present study, considering the impact of cumulative damage, the average yield point spectra are directly calculated because of the lack of elastic response spectra under seismic sequences. The proposed procedure for constructing damage-based YPS under the sequence-type ground motions that are illustrated in Fig. 2 can be summarized by the following steps.

(1) Select the damping ratio ($\zeta$) of the SDOF system and the value of $\beta$.
(2) Define the target damage level ($D_i$) and ductility capacity ($\mu_{u,j}$).
(3) Select the natural period($T$), calculate the initial stiffness of the system($K_0$).
(4) Determine the sequence-type ground motions, the elastic strength demand ($F_e$) is calculated by time history analysis.
(5) Select the strength ($\Delta F$). The yield strength ($F_y$) and yield displacement ($\Delta_y$) of the specified system can be calculated as $F_y = F_e - \Delta F$ and $\Delta_y = F_y/K_0$, respectively.
(6) Calculate the peak displacement ($\Delta_u$) and $E_h$ through elastic time history analysis. The damage index ($D$) can be calculated according to Eq. (2). The analysis is repeated for sufficient values of $\Delta F$ to develop $D$ that includes the target damage level ($D_i$) range of interest.
(7) Change the value of $T$, and repeat steps (3)–(6) to determine the spectrum that is valid for the range of $T$.
(8) Repeat steps (2)–(7) for different values of damage level and ductility factor.

A series of SDOF systems are adopted to calculate the damage-based YPS under earthquakes. The elastic–perfectly plastic (EPP) model is employed due to its simple constitutive relationship. The SDOF systems with a set of 60 periods varies from 0.1 to 6.0 s with an interval of 0.1 s are considered. Five ductility factors (i.e., $\mu_u = 2$, 4, 6, 8, and 10) and damage indices (i.e., $D = 0.1$, 0.2, 0.5, 0.8, and 1.0) are adopted to analyze different ductility performances and damage levels, respectively. The structural viscous damping ratio is assumed to be 5%.

## 5 Generation of damage-based YPS

Based on the selected 342 pairs ground motions, a total of 1 026 000 working stations are employed to obtain the average YPS with 60 periods of the SDOF system, five levels of ductility factor and damage index. The results are statistically analyzed on the basis of the period, ductility factor, damage index, site category, aftershock intensity, and structural damping. Due to the limited space, only the partial results are shown in the following sections, and other cases that have similar results are not discussed. It can be observed in Eq. 3 that $\Delta_y$ is proportional to $C_y$. The following studies therefore mainly analyze $C_y$ in the study of the YPS.

The calculated YPS of the SDOF systems with different $\mu_u$ and $D$ values under mainshocks and sequence-type ground motions with $\gamma = 0.5$ are shown in Figs. 3, 4, 5, 6. In order to analyze the influence of ground motion parameters and structural dynamic

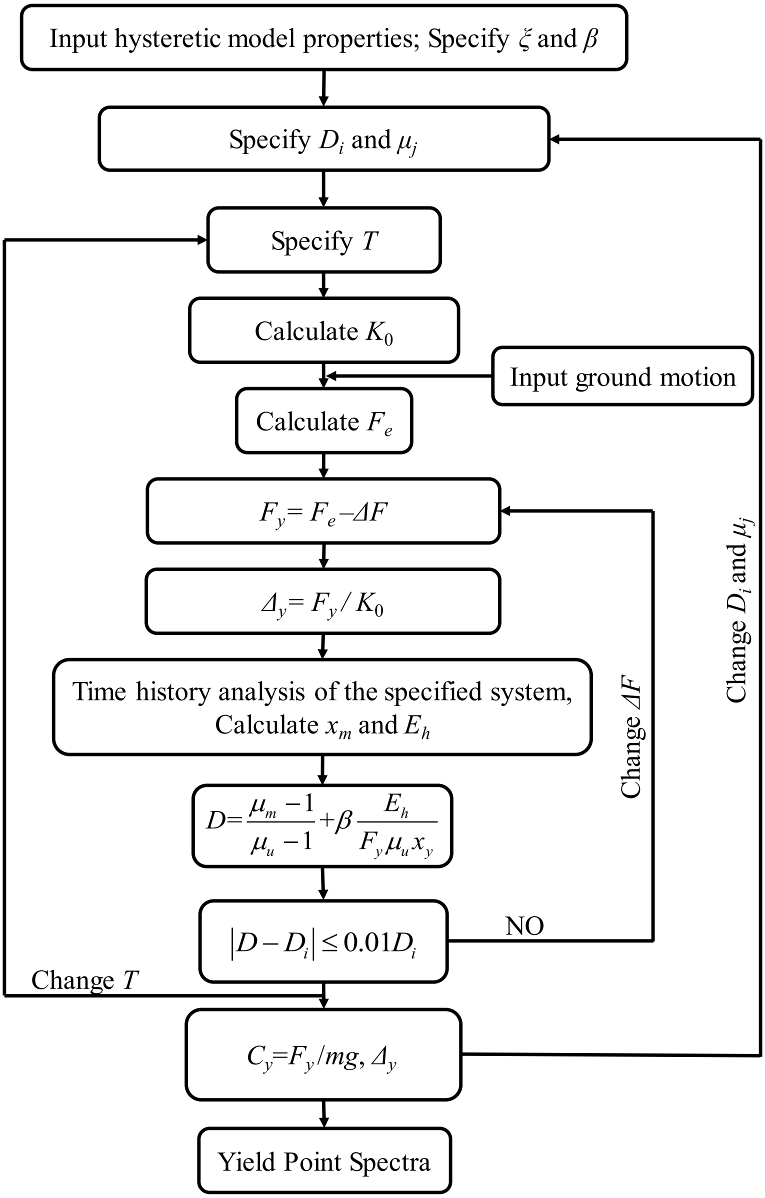


**Fig. 2** Flowchart of YPS computation

characteristics on the YPS, the YPS and $C_y$ spectra are shown in Figs. 3, 4, 5, 6a and b, respectively. It can be observed that the YPS shows the same trend which is not affected by the ductility factor, damage index, site class, and type of ground motions. In the short period region (0–0.4 s), mean $C_y$ increases sharply with increasing period. In the medium period region (0.4–2.0 s), $C_y$ decreases significantly with the increase in period.

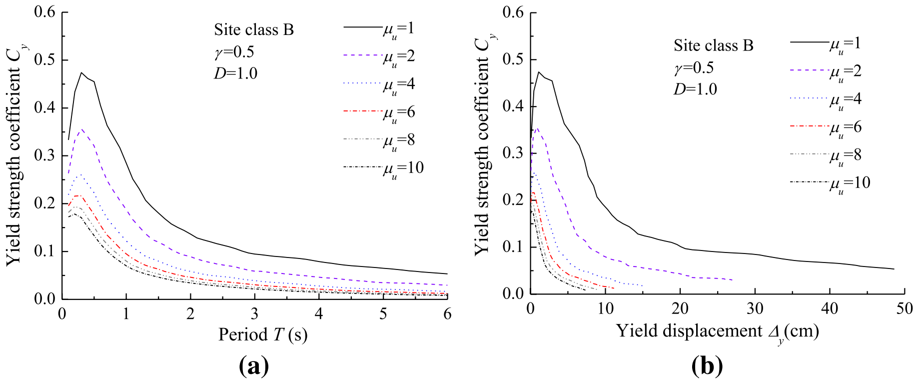


**Fig. 3** YPS on site class B, $D=1.0$, $\gamma=0.5$: **a** $C_y$ spectra, **b** YPS

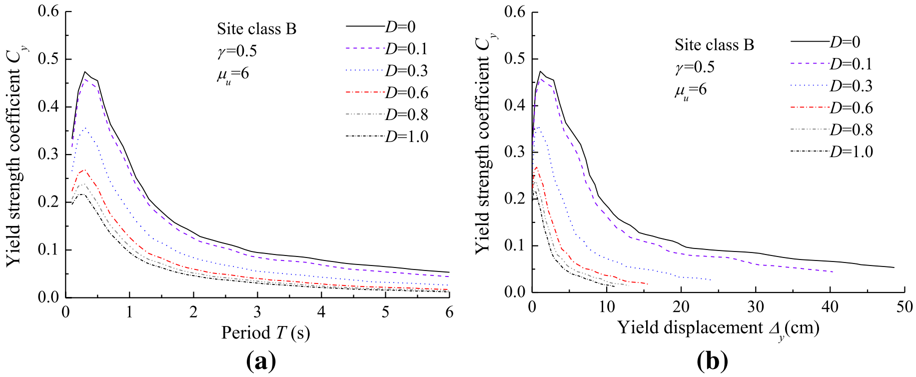


**Fig. 4** YPS on site class B, $\mu_u=6$, $\gamma=0.5$: **a** $C_y$ spectra, **b** YPS

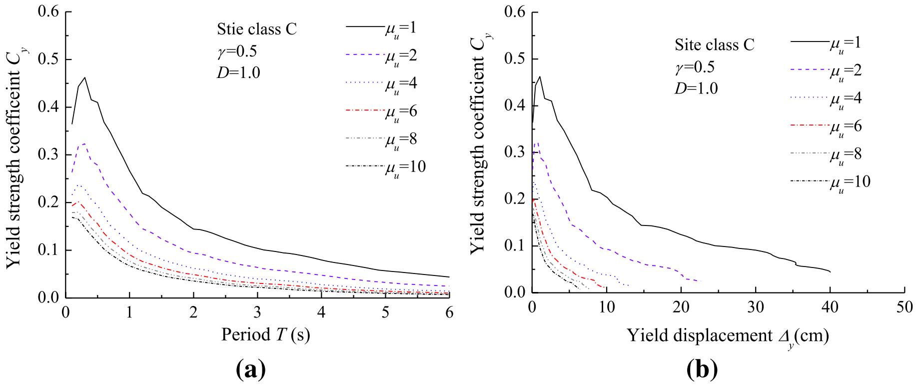


**Fig. 5** YPS on site class C, $D=1.0$, $\gamma=0.5$: **a** $C_y$ spectra, **b** YPS

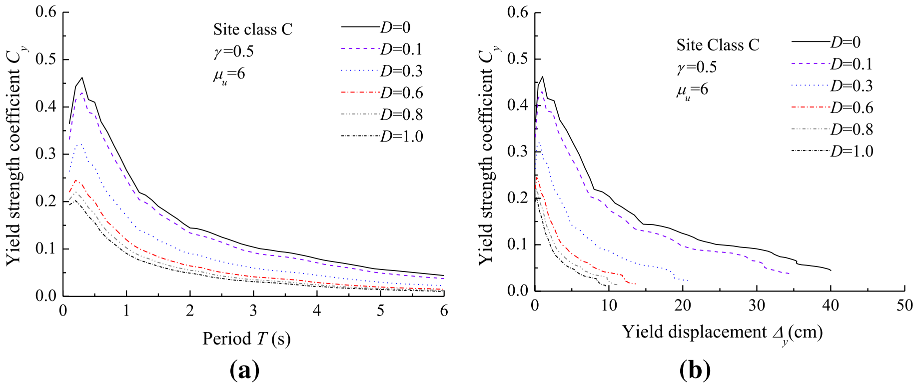


**Fig. 6** YPS on site class C, $\mu_u = 6$, $\gamma = 0.5$: **a** $C_y$ spectra, **b** YPS

The variation is gradual in the long period region (2.0–6.0 s), and $C_y$ decreases with the increasing period of systems.

In the entire period region, $C_y$ decreases with increasing $\mu_u$, that is, the structural strength demand with high ductility factor is lower than that with low ductility factor when structures are subjected to seismic sequences. This indicates that the structure with adequate ductility can effectively resist earthquakes with a certain intensity. The ductility factor has a significant effect on $C_y$. Consider $C_y$ on site class B with $D = 1.0$ as example. When structures subjected to sequence-type ground motions with $\gamma = 0.5$, the strength demand of the structure with $\mu_u = 2$ is 1.49 times the strength demand when $\mu_u = 4$ and 1.85 times when $\mu_u = 6$.

For a given $\mu_u$, $C_y$ decreases with the increase in $D$. The structural strength demand with a high damage index is lower than that with a low damage index under the same conditions. This demonstrates that the damage in the high-strength structure is less than that in the low-strength structure under sequence-type ground motions. Damage index has significant influence on structural strength demand. For example, under the condition of site class B and $\mu_u = 6$, the strength demand of the structure with $D = 0.1$ is 1.25 times of that of the structure with $D = 0.2$, and 1.85 times of the strength demand of the structure with $D = 0.5$ when subjected to sequence-type ground motion with $\gamma = 0.5$.

The yield point spectra reflect the relationship between $\Delta_y$ and $C_y$. The coefficients of variation (COV) of $\Delta_y$ and $C_y$ spectra can therefore indirectly reflect the discrete form of YPS. It can be observed from Eq. (3) that the COVs of $\Delta_y$ and $C_y$ spectra are the same. To study the extent of dispersion of YPS, the COVs of the corresponding $C_y$ spectra are computed. The COVs of $C_y$ under sequence-type ground motions with $\gamma = 0.5$ are shown in Fig. 7.

The COV increases with the increase in period, and in the relationship between the COV and ductility factor, the damage index is not evident. To some extent, it reflects the stochastic characteristics of seismic ground motion.

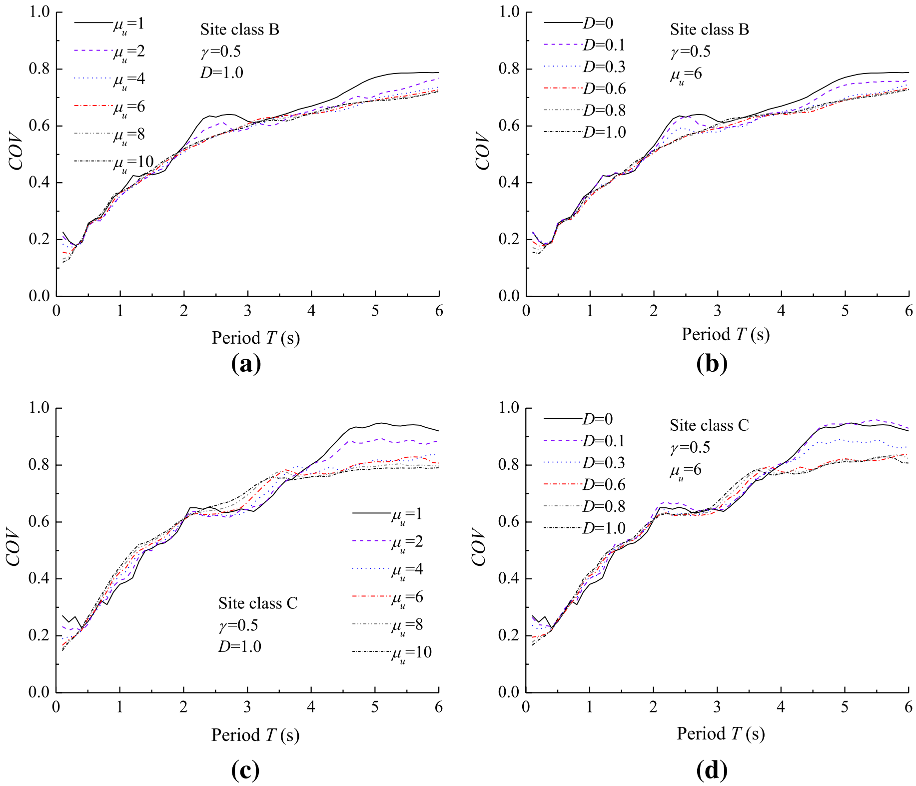


**Fig. 7** COVs of $C_y$ spectra, $\gamma = 0.5$: **a** COV on site class B, $D = 1.0$, **b** COV on site class B, $\mu_u = 6$, **c** COV on site class C, $D = 1.0$, **d** COV on site class C, $\mu_u = 6$

## 6 Effects of various parameters

### 6.1 Effect of aftershocks

The effect of aftershock on $C_y$ spectra of YPS is discussed and the computed values of $C_y$ of sequence-type ground motions and corresponding mainshocks are presented in this section. Figure 8 shows that that SDOF system's $C_y$ value increases with the increase in $\gamma$. Simply put, the stronger the aftershocks in the seismic sequence, the greater the $C_y$ value necessary for the system. For structures damaged after the mainshock, subsequent aftershocks may cause additional damage as a result of cumulative damage. In order to satisfy a given ductility factor and damage index, the structure under a seismic sequence requires a greater yield strength than that subjected only to mainshock.

In order to more clearly compare the influences of aftershock ground motions with different relative intensities ($\gamma$) on $C_y$, the ratio of $C_y$ of the sequence-type ground motion to that of the corresponding mainshock (denoted as $C_{y,seq}/C_{y,ms}$) is calculated. Figure 9 illustrates the mean $C_{y,seq}/C_{y,ms}$ for the system with $\mu_u = 6$ and $D = 1.0$ under seismic sequences with different $\gamma$ values. The $C_{y,seq}/C_{y,ms}$ increases with the increase in $\gamma$. Moreover, the influence of aftershock on the strength demands of a structure is more significant in the short period. Consider $\gamma = 1.5$ as an example. The value of $C_{y,seq}/C_{y,ms}$ reaches 1.45–1.50 in

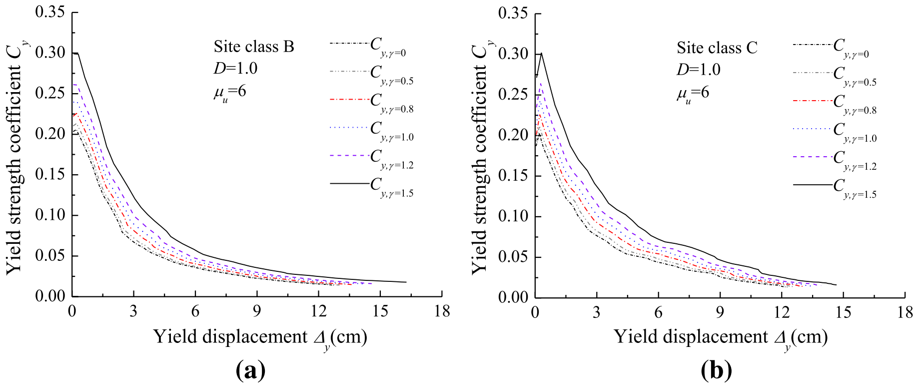


**Fig. 8** YPS with different $\gamma$ values, $\mu_u = 6$, $D = 1.0$: **a** site class *B*, **b** site class *C*

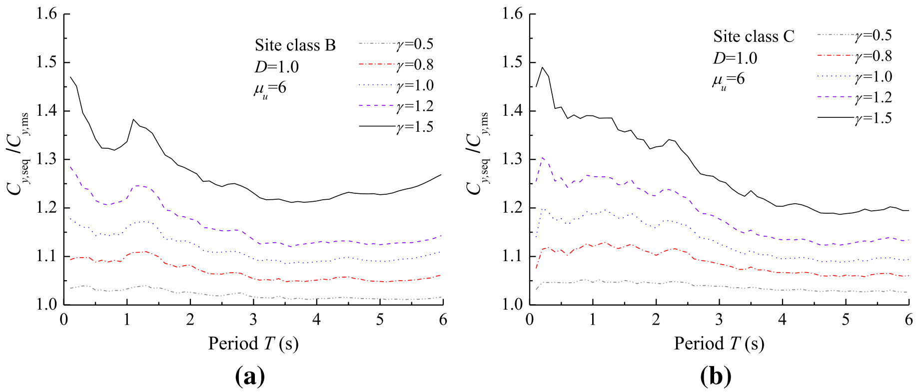


**Fig. 9** $C_{y,seq}/C_{y,ms}$ with different $\gamma$ values, $\mu_u = 6$, $D = 1.0$: **a** site class *B*, **b** site class *C*

the short period region, decreases with increasing period, and is approximately 1.25–1.30 in the long period.

When $\gamma$ is 0.5, the difference between the strength demand of the structure under a seismic sequence and that of the structure under the corresponding mainshock is less than 10%. Under this condition, the influence of aftershock on the strength demand can thus be neglected. When $\gamma$ is 1.0, the difference between the two is 10–20%, the aftershock has a considerable influence on the strength demand, and the structure that is designed without considering the influence of aftershocks is unsafe.

## 6.2 Effect of cumulative damage

To investigate the effect of cumulative damage on the YPS, the displacement ductility and modified Park–Ang model are used as indicators to measure the damage degree of structures. The ductility-based $C_{y,\mu}$ and damage-based $C_{y,D}$ under the same seismic sequence are calculated, as shown in Fig. 10. When $D$ and $\mu_u$ are the same, the trend of

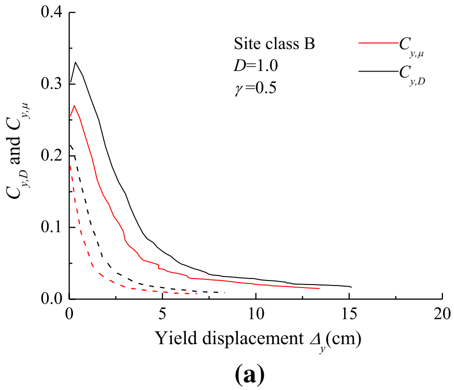


**Fig. 10** Comparison between $C_{y,D}$ ($D = 1.0$) and $C_{y,\mu}$: **a** site class B, **b** Site class C

$C_{y,D}$ and $C_{y,\mu}$ with the change in period remains basically the same. Because of the contribution of energy to structural damage, $C_{y,\mu}$ is always less than $C_{y,D}$.

To quantitatively reflect the difference between $C_{y,D}$ and $C_{y,\mu}$, $C_{y,\mu}/C_{y,D}$ with different ductility factors under seismic sequence and $\gamma = 0.5$ is studied, as shown in Fig. 11. It is indicated that the value of $C_{y,\mu}/C_{y,D}$ is 0.7–0.9 for the low ductility ($\mu_u = 2$) and 0.6–0.9 for the high ductility ($\mu_u = 6$) under sequence-type ground motions.

In short period region, the value of $C_{y,\mu}/C_{y,D}$ under sequence-type ground motions with $\gamma = 0.5$ sharply decreases with increasing period. This indicates that the proportion of the hysteresis phase in the modified Park–Ang model drastically changes. The hysteretic energy dissipation is relatively small because the structural yield strength tends to be the same as the strength demand of the elastic structure when the period approaches zero. The difference between $C_{y,\mu}$ and $C_{y,D}$ is therefore small.

In medium and long period regions, $C_{y,\mu}/C_{y,D}$ under sequence-type ground motions with $\gamma = 0.5$ slightly changes with increasing period. The reason is that the proportion of the energy phase in damage index slightly increases with increasing period. With the

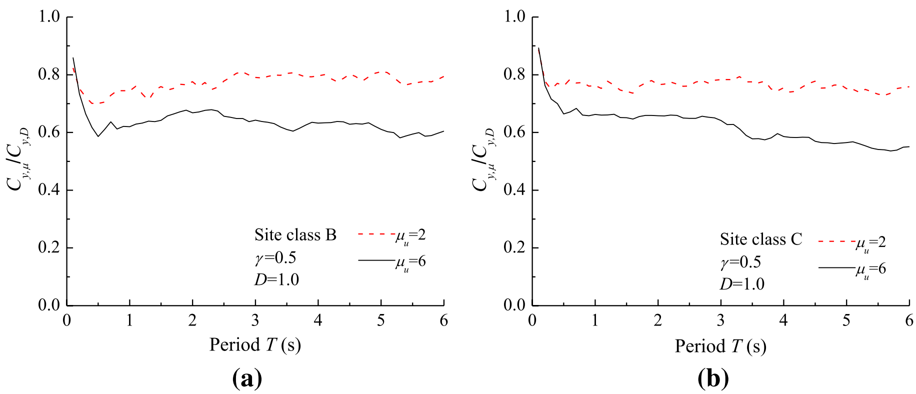


**Fig. 11** $C_{y,\mu}/C_{y,D}$ with $\gamma = 0.5$: **a** site class B, **b** site class C

increase in $\mu_u$, the hysteretic energy dissipation of the structure under seismic sequences increases, and the difference between $C_{y,\mu}$ and $C_{y,D}$ is more considerable.

### 6.3 Effect of site categories

The effect of site categories on the $C_y$ can be observed in Figs. 3, 4, 5, 6, where $C_y$ spectra are plotted under seismic sequences, which are recorded on site classes B and C. It can be seen that the spectra of $C_y$ on the two site classes have similar tendencies in whole period ranges.

For comparison, the ratio of the yield strength coefficient ($C_{y,B}$) for site class B to that of $C_{y,C}$ for site class C is calculated and plotted in Fig. 12. It can be observed that the difference between $C_{y,B}$ and $C_{y,C}$ can reach 20%. Site class B exhibits higher $C_y$ values in periods 0–1.0 s and 4.5–6.0 s, whereas it exhibits lower $C_y$ values in the period 1.0–4.5 s. This means that when the local site effect is neglected, a certain overestimation of the yield strength demand ($C_{y,B}$) results in periods 0–1.0 s and 4.5–6.0. A trend opposite the foregoing, however, is exhibited by $C_{y,C}$. It is thus evident, that impact of site conditions should be considered in seismic design. It is further observed that $C_{y,B}/C_{y,C}$ is relatively independent from ductility and damage index.

### 6.4 Effect of damping

To study the damping effect, the $C_y$ values with damping ratios of $\zeta = 0.02$ and $\zeta = 0.10$ are calculated. The $C_y$ values of these systems are normalized by the $C_y$ values with damping ratio 0.05. Figure 13 presents the mean normalized $C_y$ values of sequence-type ground motions with $\gamma = 0.5$ for each $\mu_u$ and $D$.

It can be observed that the increase in damping ratio always results in the decrease in $C_y$ by various extents. For elastic structures, the input energy of earthquake is dissipated mainly through damping. And for inelastic structures, in addition to damping, hysteretic energy is also an important factor to dissipate the input energy of earthquake. As damping increases, the damping energy also increases, and the displacement response

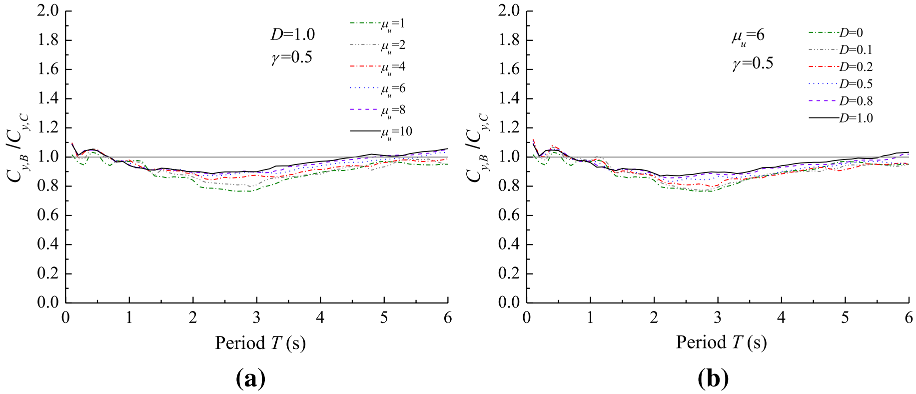


**Fig. 12** Effect of site class on YPS with $\gamma = 0.5$: **a** $C_{y,B}/C_{y,C}$, $D = 1.0$, **b** $C_{y,B}/C_{y,C}$, $\mu_u = 6$

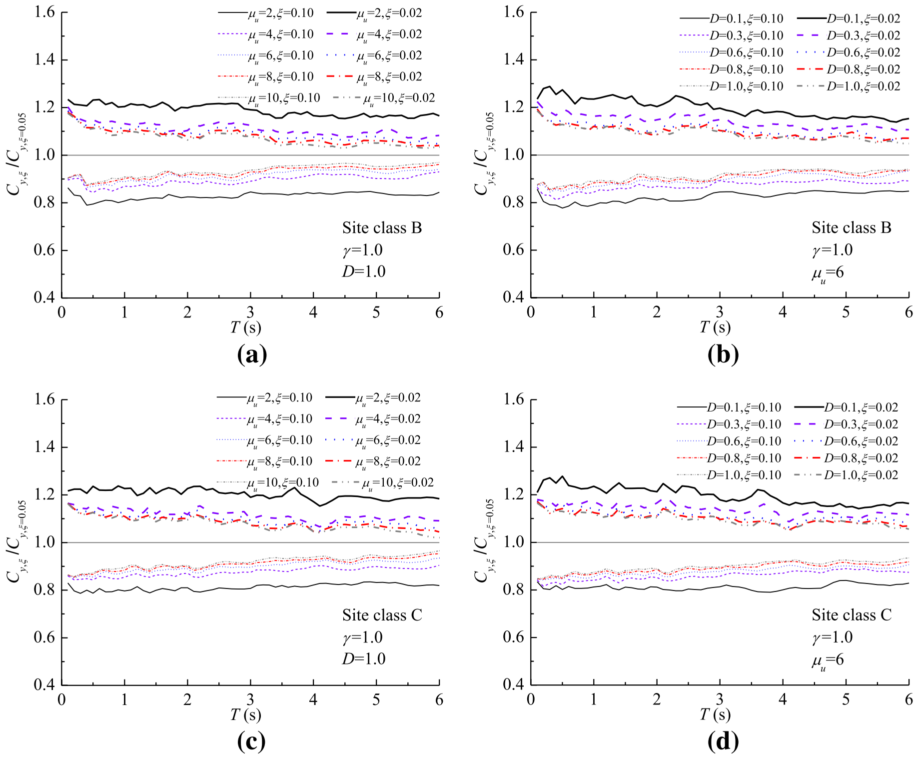


**Fig. 13** $C_{y,\zeta}/C_{y,\zeta=0.05}$ with $\gamma=0.5$: **a** $D=1.0$, site class B, **b** $\mu_u=6$, site class B, **c** $D=1.0$, site class C, **d** $\mu_u=6$, site class C

and hysteretic energy of structures subjected to the same ground motions decrease. Damping has a considerable effect on elastic structures but a minimal effect on inelastic structures.

Consider the $C_y$ value of a structure with $\zeta=0.05$ as benchmark. The influence levels of damping are typically 30% and 23% when $\zeta=0.02$ and 0.10, respectively. With the decrease in ductility factor and damage index, the corresponding $C_y$ when $\zeta=0.02$ or 0.10 approaches the $C_y$ value when $\zeta=0.05$.

### 6.5 Effect of post-yield stiffness

In order to investigate the influence of post-yield stiffness ratio ($H$) on $C_y$, the $C_y$ values of systems with $H=0.05$ and 0.1 are calculated. Thereafter, these $C_y$ values are normalized by the EPP system $C_y$ for each sequence-type ground motion. Finally, the mean normalized $C_y$ of all sequence-type ground motions with a constant $\gamma$ value is calculated for each period.

Figure 14 shows the mean normalized $C_y$ of sequence-type ground motions with $\gamma=0.5$. It can be observed that the EPP system $C_y$ is 1.0–1.1 times the $C_y$ value of the system with $H=0.05$. The $C_y$ value of the latter is 1.0–1.05 times the $C_y$ value of the system with $H=0.10$. The results indicate that although an increase in this ratio leads to a slight increase in $C_y$, it is not the major influencing factor.

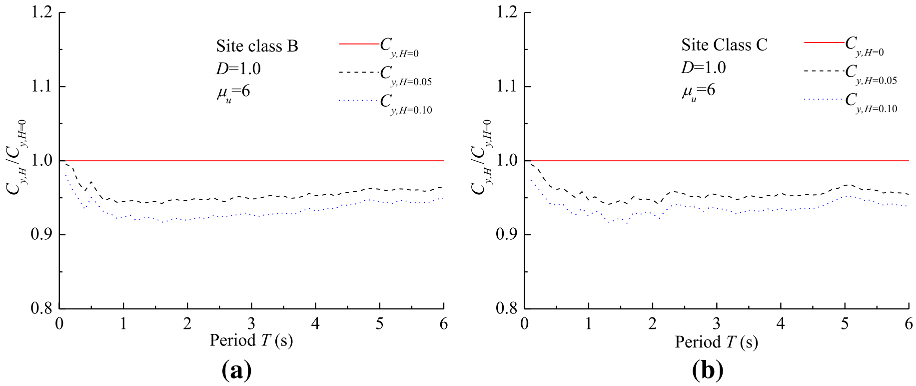


**Fig. 14** YPS with different post-yield stiffness ratios with $\gamma = 0.5$: **a** $C_{y,H}/C_{y,H=0}$, site class B, **b** $C_{y,H}/C_{y,H=0}$, site class C

## 7 Predictive model

The predictive model of the YPS is an effective tool in seismic design for determining the capacity demand of structures subjected to seismic sequences. According to the statistical results, the factors that affect the YPS are period, ductility factor, damage index, aftershock intensity, site, and damping ratio. These factors are therefore also included in the predictive model of YPS:

$$C_{ye} = \begin{cases} \left(b_0 + b_1 T\right)\eta_\gamma \eta_\zeta, & T \le 0.2s \\ \text{linear interpolation}, & 0.2s < T \le 0.4s \\ \frac{1}{b_2 + b_3 T^{1.1}}\eta_\gamma \eta_\zeta, & 0.4s < T \le 6.0s \end{cases} \tag{4}$$

$$R_D = 1 + \frac{D(\mu - 1)(a_0 T + a_0 T^2)}{(\mu + a_2)(1 + a_3 T + a_4 T^2)} \cdot \frac{1}{0.87 + 0.08e^r} \tag{5}$$

$$C_y = \frac{C_{ye}}{R_D} \tag{6}$$

$$x_y = \frac{T^2 C_y g}{4\pi^2} \tag{7}$$

where $T$ is the period; $\mu$ is the ductility factor; $D$ is the damage index; $C_{ye}$ is the pseudo-acceleration response spectra for sequence-type ground motions; $C_y$ is the yield strength coefficient; $R_D$ is the damage-based strength reduction factor, which can be obtained from the research of Sun C X et al. (2016) and Zhang et al. (2017); parameters $a_0$–$a_4$ are found in literature (Zhang et al. 2017); $\eta_\zeta$ is the damping ratio influence factor expressed as

$$\eta_\zeta = 1 + \frac{0.05 - \zeta}{0.16 + 3.2\zeta} \tag{8}$$

where $\zeta$ denotes damping; $\eta_\gamma$ is the influence factor of the aftershock intensity expressed as

**Table 3** Values of $b_0$–$b_3$

| Parameters | $b_0$ | $b_1$ | $b_2$ | $b_3$ |
|---|---|---|---|---|
| Site class B | 0.37 | 0.75 | 0.99 | 2.28 |
| Site class C | 0.29 | 1.25 | 1.08 | 2.13 |

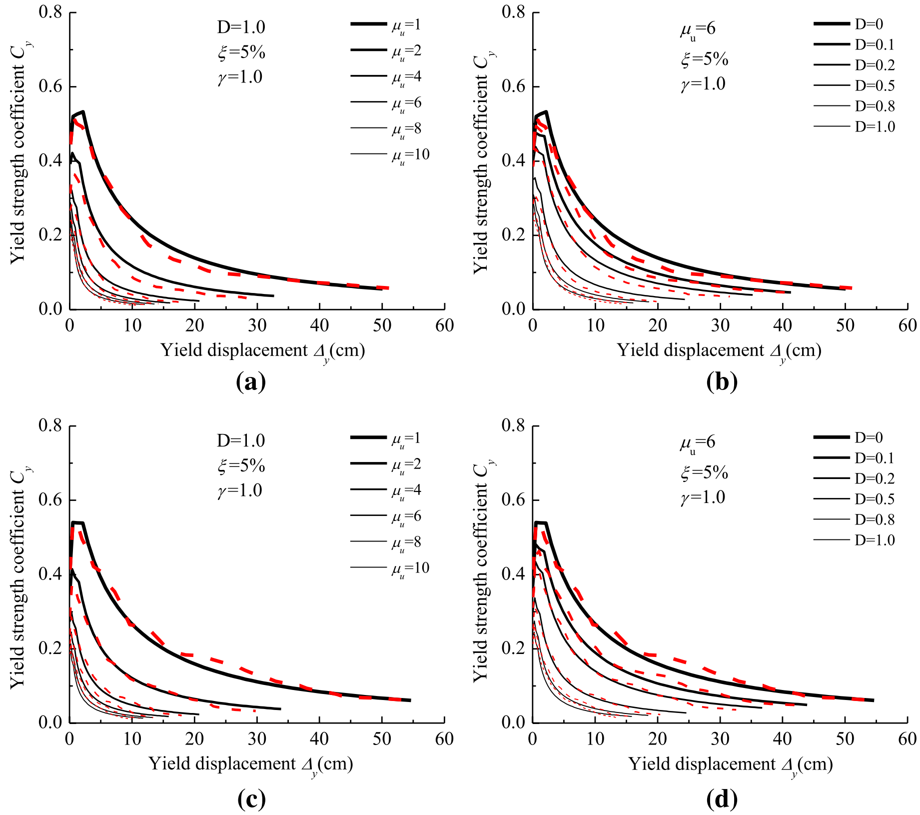


**Fig. 15** Comparison of calculated modified YPS with original spectra with $\gamma = 1.0$: **a** $D = 1.0$, site class *B*, **b** $\mu_u = 6$, site class B, **c** $D = 1.0$, site class C, **d** $\mu_u = 6$, site class C

$$\eta_\gamma = 0.93 + 0.07\gamma^{2.5} \tag{9}$$

where $\gamma$ is the relative intensity of aftershock.

The statistical data of YPS are used for the regression analysis. Parameters $b_0$, $b_1$, $b_2$, and $b_3$, which are calculated by a nonlinear least square regression analysis method, are regression parameters that depend on site classes. Table 3 summarizes the calculated values of these regression parameters.

The yield point spectra, which are predicted using Eq. (4) – (7), are compared with recorded mean spectra with $\gamma = 1.0$, as shown in Fig. 15. All ductility factors and damage indices are in good agreement.

## 8 Conclusions

The objective of this paper is to propose the damage-based yield point spectra (YPS) for mainshock-aftershock sequence-type ground motions. In the case of considering cumulative damage, the strength demands of inelastic systems can be determined more reasonably by damage-based YPS which determined for different damage indexes and ductility factors. A statistical study of the YPS is accordingly conducted. The yield point spectra are calculated for a series of elastic–plastic SDOF systems with various damage indices and ductility factors and subjected to 342 seismic sequences recorded under different site classes. In particular, the effect of aftershocks on the YPS is studied. The conclusions are as follows:

1. The yield point spectra in the short and medium period regions are strongly dependent on the period, whereas those in the long period are relatively independent from the period. In the entire period region, the yield point spectra decrease with increasing damage index ($D$) and ductility factor ($\mu_u$).
2. There is a big difference between damage-based YPS and ductility-based YPS. The former is 40% higher than the latter in the long period with $\mu_u=6$ and $\gamma=0.5$. The yield strength coefficient demand of $C_{y,D}$ is greater than that of $C_{y,\mu}$.
3. The influence of aftershock on the YPS increases with increasing aftershock intensity. The aftershock with $\gamma=0.5$ has a negligible effect on YPS, while the aftershock with $\gamma=0.5$ can increase the YPS to a 50% in the short period region. The effect of aftershock ground motion on the YPS depends on structural period, ductility factor, damage index, and aftershock intensity.
4. The predictive model of damage-based YPS is put forward, which is a function of period, ductility factor, damage index, damping, and aftershock intensity. The parameters in model are rely on site classes and hysteretic models. The predictive model can provide a good estimate of the damage-based YPS.

**Acknowledgements** The authors would like to acknowledge the support from the National Natural Science Foundation of China (Grant No. U1711264), and Shanghai Jianfeng Yichang Engineering Technology Co., Ltd.

## References

Aschheim M, Black EF (2000) Yield point spectra for seismic design and rehabilitation. Earthq Spectra 16:317–336

Aschheim M (2002) Seismic design based on the yield displacement. Earthq Spectra 18:581–600

Chopra AK, Goel RK (1999) Capacity-demand-diagram methods based on inelastic design spectrum. Earthq Spectra 15:637–656

Chopra AK, Goel RK (2001) Direct displacement-based design: use of inelastic vs. elastic design spectra. Earthq Spectra 17:47–64

Chen H, Xie Q, Li Z, Xue W, Liu K (2016) Seismic damage to structures in the 2015 Nepal earthquake sequences. Earthq Eng Eng Vib 15:173–186

Efraimiadou S, Hatzigeorgiou GD, Beskos DE (2013) Structural pounding between adjacent buildings subjected to strong ground motions. Part ii: the effect of multiple earthquakes. Earthq Eng Struct Dyn 42:1529–1545

Fajfar P (2000) A nonlinear analysis method for performance-based seismic design. Earthq Spectra 16:573–592
Freeman SA (1978) Prediction of response of concrete buildings to severe earthquake motion. Publication SP-55, American Concrete Institute, Detroit, pp 589–605
Goda K, Taylor CA (2012) Effects of aftershocks on peak ductility demand due to strong ground motion records from shallow crustal earthquakes. Earthq Eng Struct Dyn 41:2311–2330
Goda K, Salami MR (2014) Inelastic seismic demand estimation of wood-frame houses subjected to mainshock-aftershock sequences. Bull Earthq Eng 12:855–874
Hatzigeorgiou GD, Beskos DE (2009) Inelastic displacement ratios for SDOF structures subjected to repeated earthquakes. Eng Struct 31:2744–2755
Hatzigeorgiou GD (2010a) Behavior factors for nonlinear structures subjected to multiple near-fault earthquakes. Comput Struct 88:309–321
Hatzigeorgiou GD (2010b) Ductility demand spectra for multiple near- and far-fault earthquakes. Soil Dyn Earthq Eng 30:170–183
Hatzigeorgiou GD, Liolios AA (2010) Nonlinear behaviour of RC frames under repeated strong ground motions. Soil Dyn Earthq Eng 30:1010–1025
Kazama M, Noda T (2012) Damage statistics (summary of the 2011 off the pacific coast of Tohoku earthquake damage). Soils Found 52:780–792
Kotsoglou AN, Pantazopoulou SJ (2009) Assessment and modeling of embankment participation in the seismic response of integral abutment bridges. Bull Earthq Eng 7:343–361
Kowalsky MJ, Priestley MJN, Macrae GA (2010) Displacement-based design of RC bridge columns in seismic regions. Earthq Eng Struct Dyn 24:1623–1643
Kunnath SK, Reinhorn AM, Lobo RF (1992) IDARC version 3.0: A program for the inelastic damage analysis of reinforced concrete structures. Report No. NCEER-92–0022, National Center for Earthquake Engineering Research, State University of New York at Buffalo
Li Q, Ellingwood BR (2010) Performance evaluation and damage assessment of steel frame buildings under main shock-aftershock earthquake sequences. Earthq Eng Struct Dyn 36:405–427
Lu Y, Wei J (2008) Damage-based inelastic response spectra for seismic design incorporating performance considerations. Soil Dyn Earthq Eng 28(7):536–549
Moehle JP (1992) Displacement-based design of RC structures subjected to earthquakes. Earthq Spectra 8:403–428
Moon L, Dizhur D, Senaldi I, Derakhshan H, Griffith M, Magenes G, Ingham J (2014) The demise of the URM building stock in Christchurch during the 2010–2011 Canterbury earthquake sequence. Earthq Spectra 30:253–276
National Research Institute for Earth Science and Disaster Resilience (2018) Strong-motion seismograph networks (K-NET, KiK-net). https://www.kyoshin.bosai.go.jp/. Last accessed 31 December 2018
Nazari N, Van de Lindt JW, Li Y (2015) Effect of mainshock-aftershock sequences on wood frame building damage fragilities. J Perform Construct Facil 29:04014036
Negro P (1997) Experimental assessment of the global cyclic damage of framed R/C structures. J Earthq Eng 1:543–562
Pacific Earthquake Engineering Research Centre (2018) PEER ground motion database. https://ngawest2.berkeley.edu/. Accessed 13 Dec 2018
Park YJ, Ang AH (1985) Mechanistic seismic damage model for reinforced concrete. J Struct Eng 111:722–739
Powell GH (2008) Displacement-based seismic design of structures. Earthq Spectra 24:555–557
Raghunandan M, Liel AB, Luco N (2015) Aftershock collapse vulnerability assessment of reinforced concrete frame structures. Earthq Eng Struct Dyn 44:419–439
Rossetto T, Elnashai A (2005) A new analytical procedure for the derivation of displacement-based vulnerability curves for populations of RC structures. Eng Struct 27:397–409
Ruiz-García J, Negrete-Manriquez JC (2011) Evaluation of drift demands in existing steel frames under as-recorded far-field and near-fault mainshock–aftershock seismic sequences. Eng Struct 33:621–634
Safar M, Ghobarah A (2008) Inelastic response spectrum for simplified deformation-based seismic vulnerability assessment. J Earthquake Eng 12:222–248
Shen J, Ren X, Zhang Y, Chen J (2019) Nonlinear dynamic analysis of frame-core tube building under seismic sequential ground motions by a supercomputer. Soil Dyn Earthq Eng 124:86–97
Sun CX, Chen J, Zhang YQ (2016) Damage-based strength reduction factor for sequence-type ground motions. In: The 2016 structure congress, 28 August–1 September, 2016, Jeju Island, Korea
Tabatabaei R, Rahmanian MR (2012) Application of the yield point spectra (YPS) method in performance design of steel and reinforced concrete frames. J Civil Eng Res 2:18–24

Tjhin TN, Aschheim MA, Wallace JW (2007) Yield displacement-based seismic design of RC wall buildings. Eng Struct 29:2946–2959

Wang Z (2008) A preliminary report on the great Wenchuan earthquake. Earthq Eng Eng Vib 7:225–234

Zhai CH, Wen WP, Li S, Xie LL (2015) The ductility-based strength reduction factor for the mainshock–aftershock sequence-type ground motions. Bull Earthq Eng 13:2893–2914

Zhai CH, Wen WP, Chen ZQ, Li S, Xie LL (2013) Damage spectra for the mainshock–aftershock sequence-type ground motions. Soil Dyn Earthq Eng 45:1–12

Zhang Y, Chen J, Sun C (2017) Damage-based strength reduction factor for nonlinear structures subjected to sequence-type ground motions. Soil Dyn Earthq Eng 92:298–311